SCIENCE CHINA
Chemistry

• ARTICLES •

February 2016 Vol.59 No.2: 231–236
doi: 10.1007/s11426-015-5444-4

Optoeletronic investigation of $Cu_2ZnSn(S,Se)_4$ thin-films & $Cu_2ZnSn(S,Se)_4$/CdS interface with scanning probe microscopy

Jiangjun Li, Yugang Zou, Ting Chen, Jinsong Hu, Dong Wang* & Li-Jun Wan*

Beijing National Laboratory for Molecular Science; Key Laboratory of Molecular Nanostructure and Nanotechnology; Institute of Chemistry, Chinese Academy of Sciences, Beijing 100190, China

Received April 13, 2015; accepted May 4, 2015; published online July 31, 2015

The kesterite-structured semiconductor $Cu_2ZnSn(S,Se)_4$ (CZTSSe) is prepared by spin coating a non-hydrazine precursor and annealing at Se atmosphere. Local electrical and optoelectronic properties of the CZTSSe thin-film are explored by Kelvin probe force microscopy and conductive atomic force microscopy. Before and after irradiation, no marked potential bending and very low current flow are observed at GBs, suggesting that GBs behave as a charge recombination site and an obstacle for charge transport. Furthermore, CdS nano-islands are synthesized via successive ionic layer adsorption and reaction (SILAR) method on the surface of CZTSSe. By comparing the work function and current flow change of CZTSSe and CdS in dark and under illumination, we demonstrate photo-induced electrons and holes are separated at the interface of p-n junction and transferred in CdS and CZTSSe, respectively.

CZTSSe, CdS, GBs, heterojunction, KPFM, c-AFM

Citation: Li J, Zou Y, Chen T, Hu J, Wang D, Wan L-J. Optoeletronic investigation of $Cu_2ZnSn(S,Se)_4$ thin-films & $Cu_2ZnSn(S,Se)_4$/CdS interface with scanning probe microscopy. *Sci China Chem*, 2016, 59: 231−236, doi: 10.1007/s11426-015-5444-4

1 Introduction

In the past decade, great attention has been focused on thin-film chalcogenide photovoltaic devices [1] due to its high power conversion efficiency (PCE) and low fabrication-cost. Because of appropriate band gap and high absorption coefficient, thin-film chalcogenide photovoltaic devices such as CdTe, $CuIn(S,Se)_2$, CISSe, $Cu(In,Ga)(S,Se)_2$ yield cell efficiencies of greater than 15% (19.6% for CdTe [2], 20.8% for CIGSSe [3]). Despite the excellent performance of CdTe and CIGSSe, their extensive application for desirable energy production is limited due to the toxic elemental composition (Cd) or scare elements in the earth's crust (Te,In,Ga). By replacing above inapposite resources with zinc and tin, Cu_2ZnSnS and $Cu_2ZnSn(S,Se)$ (CZTSSe) composed of earth-abundant, non-toxic elements have been intensively studied, leading to continuous device performance improvement and achieving PCE of up to 12.6% [4].

The most extensive work on chalcogenide photovoltaic devices has been performed on the growth of CZTS (or CZTSSe) thin film materials and corresponding device architectures. In 1997, Katagiri *et al*. [5] firstly designed a Al/ZnO/CdS/CZTS/Mo/Soda Lime Glass device, yielding a PCE of 0.66% under AM 1.5 illumination. Over the past decade, many efforts have been made to improve the crystalline quality of kesterite phase CZTS (or CZTSSe) using various deposition methods, as well as to improve device performance. Beyond sputtering and evaporation [6,7], some non-vacuum approaches such as electrodeposition [8], bath-based techniques [9,10], spray pyrolysis [11], ink-based approaches [12,13] were developed and applied to growth of CZTS, CZTSSe photovoltaic films.

In a typical Al/ZnO/CdS/CZTS(Se)/Mo/Soda Lime Glass

*Corresponding authors (email: wangd@iccas.ac.cn; wanlijun@iccas.ac.cn)

device architecture, the n-type buffer layer CdS is applied to eliminate the band gap discrepancy and lattice mismatching between CZTS and ZnO and thus improves the devices' output performance. As the photo-induced electrons pass the CZTS (or CZTSSe)/CdS interface, the band alignment at the interface is very crucial for devices performance [14–16]. The positive conduction band offset (CBO) between CZTS (or CZTSSe) and CdS increases the open circuit voltage (V_{oc}) [17] while the barrier blocks minority (electron) transport from the absorber CZTS (or CZTSSe) to the buffer layer CdS can reduce the short circuit current (J_{sc}). Conversely, the negative CBO gives rise to interface recombination can significantly lower the V_{oc} thereby reducing the PEC of the device. Several groups have reported the band alignments for CZTS(Se)/CdS [14–16,18,19] based on X-ray photoelectron spectros-copy, optical absorption spectroscopy and first-principles calculation. In addition to the energetic alignment of the conduction band edges, the Fermi levels at the heterojunction interfaces that reflect the chemical potentials of electrons, are also useful for understanding the electronic structure, which is of paramount importance to study the photovoltaic process of inorganic solar cell devices.

Apart from traditional characterization methods for photovoltaic devices, scanning probe microscope (SPM) provides various powerful approaches to extract local morphology and electronic properties of the electrode interface. In particular, Kelvin probe force microscopy (KPFM) and conductive atomic force microscopy (c-AFM) have been broadly applied to study the phase separation, photovoltaic properties of heterojunction solar cells [20–27], electronic mapping of cross sections of solar cell devices [26,28–30], band bending at Schottky junction interfaces[31,32], as well as the surface photocatalytic activities of materials [33,34]. KPFM can determine local contact potential difference (CPD) between sample and probe by nullifying the probe's amplitude (amplitude modulation [35], AM) or frequency shift (frequency modulation [36], FM) when the compensated DC voltage is applied to tip, while topographic images are recorded simultaneously. C-AFM detects the current flowing between samples and tips in contact mode and thus shows local surface conductivity. KPFM and c-AFM have provided useful insight into deep understanding the effects of illumination, bias voltage and nanostructure on the performance of organic or inorganic solar cells. For example, using the KPFM, Jiang *et al*. [37] found that built-in potential on the grain boundaries (GBs) plays an important role in CIGS thin film solar cells' conversion efficiencies. However, for CZTSSe thin film, reports on the local electronic properties with a nanoscale resolution, especially photoelectronic characters, are seriously rare. Moreover, there is no SPM report of electric and optoelectronic structure of CZTSSe/CdS interfaces because of the cell architecture.

In this paper, we present the combined KPFM and c-AFM study of photoelectronic behavior of the kesterite-structured CZTSSe thin film at the nanoscale. We fabricated highly crystalline CZTSSe thin films via a non-hydrazine solution-based processing. A direct visualization of the carrier generation on the crystal planes under the illumination is achieved through KPFM. C-AFM measurements on the thin film under illumination and in dark demonstrate the generation of photo-current. To investigate electronic properties of the p-n junction interfaces with sub-nanometer resolution, photo-response measurements on CZTSSe film loaded with n-type CdS nanoislands via successive ionic layer adsorption and reaction (SILAR) method were carried out. Charge generation and separation were observed on the p-n junctions, thus form potential difference under open circuit condition.

2 Experimental

The growth and characterization (scanning electron microscope, X-ray diffraction, Raman spectrum) for CZTSSe thin film can be seen in Supporting Information online. Atomic force microscopy experiments were carried out in a glove box under argon atmosphere at room temperature and pressure, using a Peak Force Mode AFM (multimode 8, Bruker). KPFM measurements were performed in dark (the glove box was covered with light block curtains) and under continuous visible light (400–800 nm) illumination provided by a commercial Sun Full Spectrum Light Source (NBet, China) optical fiber at 100 mW/cm^2, which is well matched with natural spectrum in the range of visible light. Estimated irradiation power levels at the sample surface were about 30 mW/cm^2. It is worth reminding that the AFM laser has the wavelength of above 600 nm (E>2.07 eV) which is above the band gap of CZTSSe (1.1–1.5 eV). However, the intensity of laser is low and does not affect our measurements significantly. In FM-KPFM, first scan is used for topographic imaging with Peak Force Mode, then probe is lift in interleave mode and measures the CPD. For FM-KPFM, the frequency modulation (f_{mod}) applied to the tip is constant (about 2 kHz), giving rise to sidebands appearing at $f_0\pm f_{mod}$ and $f_0\pm 2f_{mod}$ around the tip's fundamental resonance peak at f_0. These sidebands originate from the modulated force gradient between tip and local sample. The amplitudes of sideband at $f_0\pm f_{mod}$ are proportional to CPD ($\phi_{tip}-\phi_{sample}$, ϕ_{tip} and ϕ_{sample} represent the work function of the tip and sample, respectively) and demodulated via Lock-In Amplifier (LIA), and then nullified by the compensating DC voltage (equal to CPD) applied to probe through the controller. Thus, the CPD is achieved along with the topographic recording. A silicon probe (force constant: 0.4–1.2 N/m, tip radius: 12 nm) is used for CPD measurement with the Lift Mode. For c-AFM, a conductive probe coated with Au is used for recording the current between sample and tip when bias voltage is applied to sample. Figure 1 shows KPFM and c-AFM setup and device structure.

3 Results and discussion

3.1 KPFM and c-AFM of CZTSSe film

Topographic image in Figure 2(a) exhibits various crystal planes on the surface of CZTSSe thin film, with a lateral crystalline dimension of several hundred nanometers. Figure 2(b) displays the topography of a small scan size, and the corresponding CPD result is showed in Figure 2(c) in dark (lower half) and under illumination (upper half). The CPD is correlated to the work function of local surface. The absolute surface work function of CZTSSe is about ~5.2 eV. Upon illumination the average value of CPD increases about 70 mV compared with that of in dark condition, indicating that the work function of CZTSSe thin film is decreased. This increase in CPD corresponds to the presence of additional positive charge carriers indicates that after illumination free charge carriers are generated, and then holes are transported to glass electrode and then the ground, while electrons are accumulated in p-type CZTSSe thin film layer, which leads to work function deceasing. In addition, the CPD values of GBs are undistinguished compared to that of adjacent crystal planes, suggesting that there is no detected band bending at GBs. The measured CPD distribution and variation before and after illumination confirm the intrinsic efficient transport of holes through CZTSSe grains.

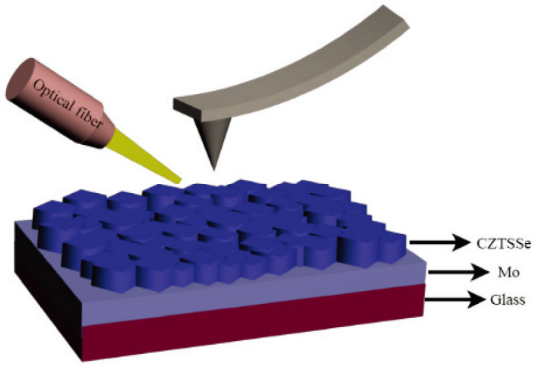

Figure 1 Schematic diagram of setup and device structure (color online).

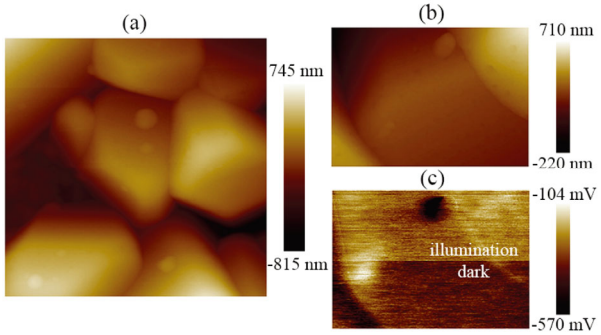

Figure 2 (a) AFM topographic image (3 μm×3 μm) of the CZTSSe film; (b) AFM topographic image (0.84 μm×1.2 μm); (c) corresponding CPD image recorded in dark (bottom half) and under illumination (upper half), as indicated by the text in white (color online).

To further investigate the role of crystal planes and GBs in collection and transport of carriers, we have performed c-AFM measurements on the CZTSSe thin film. Figure 3(a) shows the topographic image of polycrystalline CZTSSe. In combination with Peak Force Error image (Figure 3(b)), it clearly shows that conductivity of GBs is poor than that of crystal planes both in dark (Figure 3(c)) and under illumination (Figure 3(d)). Figure 4 presents the line profiles of Figure 3(c, d) that were obtained along the white lines. The dramatically increased current is located at the crystal planes under illumination while no significant change takes place at the GBs where detective current is nearly equal to zero. It means that both electrons and holes cannot be transported at GBs. Because measurements were performed at same bias voltage, the higher current mapping obtained under illumination must be a combination of injected current from bias voltage [38] and photocurrent gain [39]. The

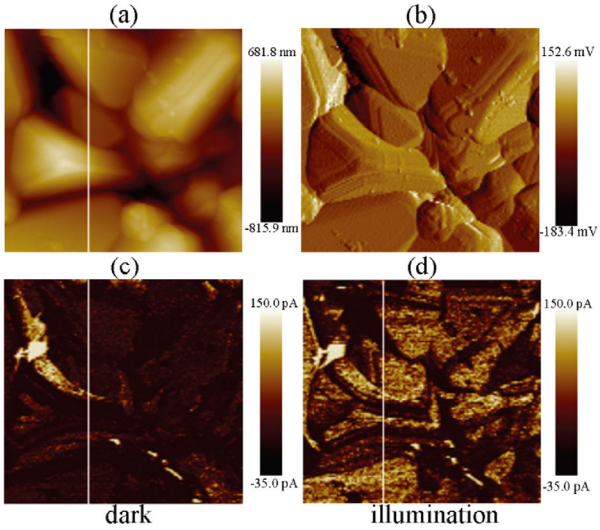

Figure 3 AFM topographic image (5 μm×5 μm) of the CZTSSe film (a) and corresponding Peak Force Error image (b); conductive atomic force microscopy image in dark (c) and under illumination (d), with a conductive gold-coated tip, sample bias voltage 4 V (color online).

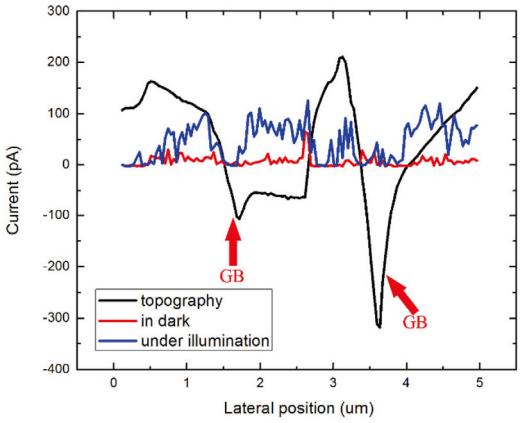

Figure 4 Current variation along the cross-section along the white lines marked in Figure 3(c, d) (color online).

photocurrent gain demonstrates the incremental carrier concentration and collection under illumination occurring at crystal planes rather than GBs. These results are inconsistent with previous literatures showing that higher current flowed through GBs [40–42]. Our observation can be attributed to that GBs act as recombination sites. Li *et al*. [43] reported that GBs create high density of localized defect state which promote the combination of photo-excited electrons and holes by first-principles calculations. Similarly, Yin *et al*. [44] suggested that wrong bonds in GBs create the defect states where the Fermi level is pinned and thus the GBs act as Shockley-Read-Hall recombination centers. Our KPFM measurements reveal that there is no change of CPD in GBs compared to the surface of the grains. These results imply that for the non-hydrazine solution-based CZTSSe thin films, the generation and transport of photo-induced carriers take place on the grains but not on GBs.

3.2 KPFM and c-AFM of CZTSSe/CdS interface

Since the finite thickness of the thin films, it is hard to directly observe the electronic properties of the cross section especially p-n junctions for CIGS, CZTS and CZTSSe solar cells. We loaded the n-type CdS quantum dots on the CZTSSe films via successive ionic layer adsorption and reaction (SILAR) method (see Supporting Information online) to expose the p-n junctions, as shown in Figure 5(a, b). By reducing the reaction time, CdS quantum dots with low coverage are loaded on the surface of grains. Due to the aggregation of CdS quantum dots, the CdS islands with diameter ranges from 20–120 nm are formed. Thus these CdS nanoparticles should have the similar electric properties compared to corresponding bulk materials. Figure 5(c) and (d) reveals the CPD measurements of p-type CZTSSe loaded with n-type CdS islands before and after illumination, respectively. The CPD of CdS is slightly lower than that of CZTSSe, implying a good Fermi level alignment exists in the interface between CZTSSe and CdS. In dark, the average CPD of the whole scan area is –0.430 V (Figure 5(a)), while under illumination, there is a shift of the CPD toward larger values, yielding an average value of –0.354 V, elucidating the presence of excess electron carriers on the surface.

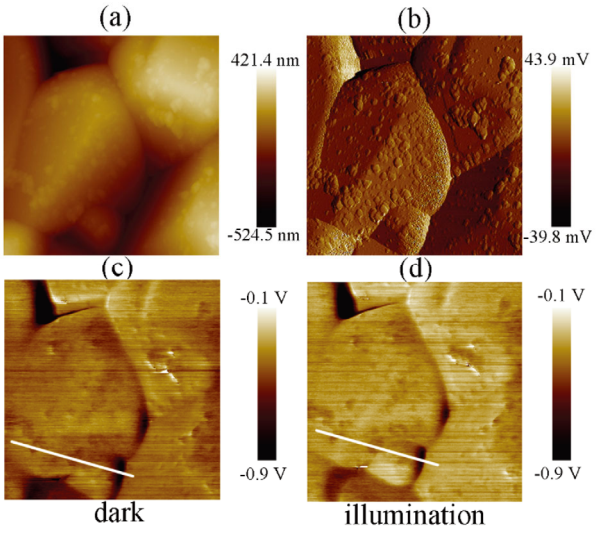

Figure 5 (a, b) AFM topographic image (2 μm×2 μm) of the CZTSSe film (a) and corresponding Peak Force Error image (b); (c, d) CPD image in dark (c) and under illumination (d), with an uncoated silicon tip (color online).

To clearly reveal the CPD change occurred on CdS, the CPD variation cross-section along white lines marked in Figure 5(c, d) is reproduced in Figure 6. The sunken positions in the CPD curve marked by red arrows correspond to the two CdS islands. It is obviously found that the CPD of CdS also increases after illumination. In addition, the difference of CPD between CZTSSe and CdS under illumination is much higher than (about 30 mV) that of in dark condition, as see the darker contrast in Figure 5(d), which means CZTSSe is more electronegative than CdS. The wavelength of incident visible light is below the band gap of CdS (about 2.4 eV). On the other hand, the intensity of the incident light is low. Therefore, the CdS cannot be excited significantly. KPFM were performed under the condition of open circuit. Therefore electrons cannot be transferred to probe. This suggests that after generation of photo-induced electrons and holes, holes are transported from CZTSSe to the Mo/glass electrode while electrons are accumulated on CZTSSe. After illumination the more electronegative CZTSSe compared with CdS reveals a small percentage of photo-electrons are transported to CdS. In other word, a low barrier exists in the conduction band edges between CZTSSe and CdS, as shown in the band alignment and charge transfer model in Figure 7 (assume the CBO is positive). Our observations agree with the fact that n-type CdS blocks holes but separates and collects electrons. It is the first time to directly observe electronic properties and photovoltaic effect process for CZTSSe/CdS heterojunction in the nanometer range.

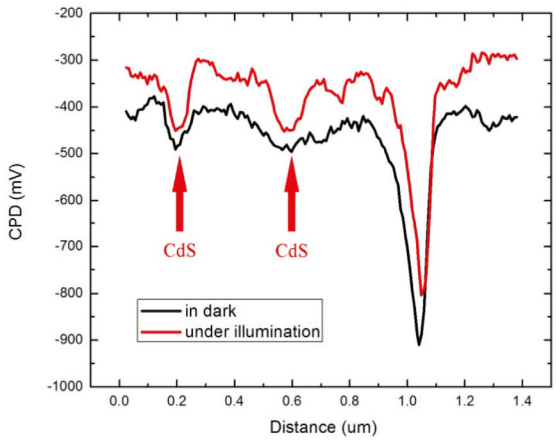

Figure 6 CPD variation along the cross-section along the white lines marked in Figure 5(c, d) (color online).

Finally, we also closely performed c-AFM measurements on CZTSSe thin-film loaded with CdS, as depicted in Figure 8. Figure 8(c) reveals the current flow from to sample to probe under relatively large bias voltage (2.5 V). With no illumination, the current flow through CZTSSe and CdS reaches several pAs. In contrast to the dark condition, we found that for the same bias voltage the current going through the CZTSSe and CdS increased steeply under illumination due to photo-induced electrons and holes as shown in Figure 8(c, d). As discussed above, the higher current flow through CdS islands compared to the dark condition indicates that excess electrons come from CZTSSe layer. Moreover, under illumination, the current through the CZTSSe distinctly exceeds that through CdS islands. At positive sample bias voltages, holes are transported from CZTSSe to high work function Au-coated tip, while electrons are transported to from CdS to CZTSSe, finally to glass electrode. It is generally known that CdS layer block holes transfer. Thus the lower current flow through CdS islands stem from relatively low electron concentration. At a large positive bias applied to sample electrons injections from tip contributes to detect current at V=2.5 V. At such a condition, the observed current also should be a combination of photocurrent gain and injected current under illumination. Under light exposure, photo-induced holes and electrons are collected and transferred by CZTSSe and CdS respectively, resulting in current increasing greatly under the same bias compared to the dark condition. Our c-AFM experimental results are well consistent with KPFM measurements.

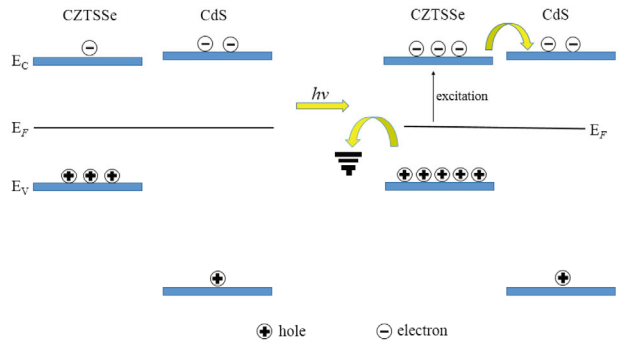

Figure 7 Schematic diagram of band alignment of a CZTSSe/CdS interface before and after illumination (color online).

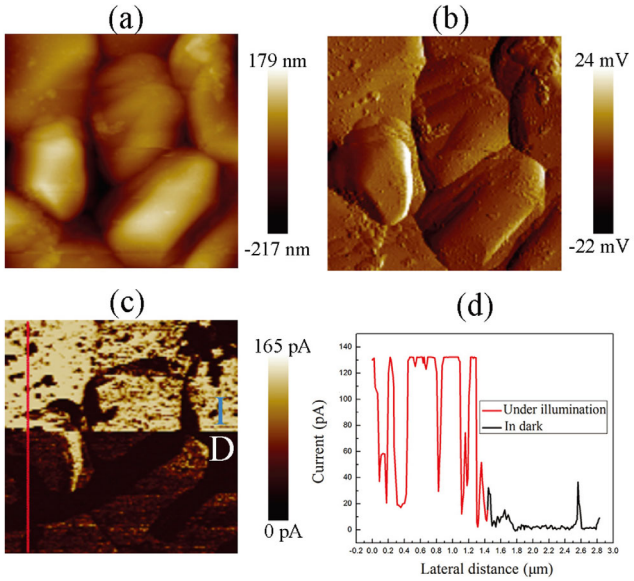

Figure 8 (a, b) AFM topographic image (3 μm×3 μm) of the CZTSSe film loaded CdS (a) and corresponding Peak Force Error image (b); (c) conductive atomic force microscopy image in dark (half bottom, as indicated by the word D in white) and under illumination (half upper, as indicated by the word I in blue), with a conductive gold-coated tip, sample bias voltage 2.5 V; (d) the variation along the cross-section along the red lines marked in (c) (color online).

4 Conclusions

In summary, we have demonstrated the applications of KPFM and c-AFM for nanoscale characterization of solution-processed kesterite solar cells thin-film materials. For the non-hydrazine route synthesized CZTSSe thin-film, KPFM and c-AFM measurements confirm the photovoltaic effect of crystalline grains. At the same time, GBs reveal non-conspicuous difference in work function and very low electrical conductivity compared to grains. The two measurements illustrate holes and electrons are collected and transferred directly in grains rather than GBs that are almost inevitably acting as recombination centers due to the existence of defects. After growth of n-type CdS on p-type CZTSSe thin-film, we can observe directly that holes are collected and transferred through CZTSSe while minority electrons are collected by CdS under illumination by KPFM measurements. A low conduction barrier exists in the CZTSSe/CdS interface. In the c-AFM studies, the drastic increasing of current gain under illumination at bias voltage occurring both at CZTSSe and CdS also confirms the effective charge separation taking place at the p-n junction interface. The present work demonstrates that direct microscopic study of optoelectronic characterization of p-n junction can help understanding local properties of polycrystalline thin-film photovoltaic materials, which is pivotally important for the engineering of hetero-junction structures in solar cells.

Acknowledgments This work was supported by the National Basic Research Program of China (2011CB932301, 2011CB808704), the National Natural Science Foundation of China (21127901, 21373236), and the Strategic Priority Research Program of the Chinese Academy of Sciences (XDB12020100)..

Conflict of interest The authors declare that they have no conflict of interest.

Supporting information The supporting information is available online at *chem.scichina.com* and *link.springer.com/journal/11426*. The supporting materials are published as submitted, without typesetting or editing. The responsibility for scientific accuracy and content remains entirely with the authors.

1 Mitzi DB, Gunawan O, Todorov TK, Wang K, Guha S. *Sol Energ Mat Sol C*, 2011, 95: 1421–1436
2 Green MA, Emery K, Hishikawa Y, Warta W, Dunlop ED. *Prog Photovolt*: *Res Appl*, 2013, 21: 827–837
3 Jackson P, Hariskos D, Wuerz R, Wischmann W, Powalla M. *Phs Status Solidi RRL*, 2014, 8: 219–222
4 Wang W, Winkler MT, Gunawan O, Gokmen T, Todorov TK, Zhu Y, Mitzi DB. *Adv Energy Mater*, 2014, 4: 1301465
5 Katagiri H, Sasaguchi N, Hando S, Hoshino S, Ohashi J, Yokota T. *Sol Energy Mater Sol Cells*, 1997, 49: 407–414
6 Zoppi G, Forbes I, Miles RW, Dale PJ, Scragg JJ, Peter M. *Prog Photovolt*: *Res Appl*, 2009, 17: 315– 319
7 Wang K, Gunawan O, Todorov T, Shin B, Chey SJ, Bojarczuk NA, Mitzi D, Guha S. *Appl Phys Lett*, 2010, 97: 143508
8 Scragg JJ, Dale PJ, Peter LM, Zoppi G, Forbes I. *Phys Status Solidi B*, 2008, 245: 1772–1778
9 Moriya K, Tanaka K, Uchiki H. *J Appl Phys*, 2005, 44: 715–717
10 Moriya K, Watabe J, Tanaka K, Uchiki H. *Phys Status Solidi C*, 2006, 3: 2848–2852
11 Nakayama N, Ito K. *Surf Sci*, 1996, 92: 171–175
12 Todorov T, Kita M, Carda J, Escribano P. *Thin Solid Films*, 2009, 517: 2541–2544
13 Steinhagen C, Panthani MG, Akhavan V, Goodfellow B, Koo B, Korgel BA. *J Am Chem Soc*, 2009, 131: 12554–12555
14 Haight R, Barkhouse A, Gunawan O, Shin B, Copel M, Hopstaken M, Mitzi DB. *Appl Phys Lett*, 2011, 98: 253502
15 Chen S, Yang JH, Gong XG, Walsh A, Wei SH. *Phys Rev B*, 2010, 81: 245204
16 Nagoya A, Asahi R, Kresse G. *J Phys Condens Matter*, 2011, 23: 404203
17 Gloeckler M, Sites JR. *Thin Solid Films*, 2005, 480: 241–245
18 Bär M, Schubert BA, Marsen B, Wilks RG, Pookpanratana S, Blum M, Krause S, Unold T, Yang W, Weinhardt L, Heske C, Schock HW. *Appl Phys Lett*, 2011, 99: 222105
19 Dong ZY, Li YF, Yao B, Ding ZH, Yang G, Deng R, Fang X, Wei ZP, Liu L. *J Phys D*: *Appl Phys*, 2014, 47: 075304
20 Xin H, Reid OG, Ren G, Kim FS, Ginger DS, Jenekhe SA. *ACS Nano*, 2010, 4: 1861–1872
21 Kamkar DA, Wang M, Wudl F, Nguyen TQ. *ACS Nano*, 2012, 6: 1149–1157
22 Hamadani BH, Jung SY, Haney PM, Richter LJ, Zhitenev NB. *Nano Lett*, 2010, 10: 1611–1617
23 Ellison DJ, Kim JY, Derek M, Stevens C, Frisbie D. *J Am Chem Soc*, 2011, 133: 13802–13805
24 Douhéret O, Lutsen L, Swinnen A, Breselge M, Vandewal K, Goris L, Manca J. *Appl Phys Lett*, 2006, 89: 032107
25 Spadafora EJ, Demadrille R, Ratier B, Grévin B. *Nano Lett*, 2010, 10: 3337–3342
26 Zeng TW, Ho CC, Tu YC, Tu GY, Wang LY, Su WF. *Langmuir*, 2011, 27: 15255–15260
27 Kong J, Lee J, Jeong Y, Kim M, Kang SO, Lee K. *Appl Phys Lett*, 2012, 100: 213305
28 Visoly-Fisher I, Cohen SR, Cahen D, Ferekides CS. *Appl Phys Lett*, 2003, 83: 4924–4926
29 Lee J, Kong J, Kim H, Kang SO, Lee K. *Appl Phys Lett*, 2011, 99: 243301
30 Bergmann VW, Weber SAL, Ramos FJ, Nazeeruddin MK, Grätzel M, Li D, Domanski AL, Lieberwirth I, Ahmad S, Berger R. *Nat Commun*, 2014, 5: 5001
31 Koren E, Berkovitch N, Azriel O, Boag A, Rosenwaks Y, Hemesath ER, Lauhon LJ. *Appl Phys Lett*, 2011, 99: 223511
32 Ishii H, Hayashi N, Ito E, Washizu Y, Sugi K, Kimura Y, Niwano M, Ouchi Y, Seki K. *Phys Status Solidi A*, 2004, 201: 1075–1094
33 Wu MC, Liao HC, Cho YC, Hsu CP, Lin TH, Su WF, Spi A, Kukovecz A, Konya Z, Shchukarev A, Sarkar A, Larsson W, Mikkola JP, Mohl M, Toth G, Jantunen H, Valtanen A, Huuhtanen M, Keiski RL, Kordas KJ. *J Nanopart Res*, 2013, 16: 1–11
34 Wang G, Yan Y, Yang X, Li J, Qiao L. *Electrochem Commun*, 2013, 35: 100–103
35 Palermo V, Palma M, Samorì P. *Adv Mater*, 2006, 18: 145–164
36 Dominik Z, Andreas S. *Nanotechnol*, 2011, 22: 075501
37 Jiang CS, Noufi R, Ramanathan K, AbuShama J, Moutinho H, Al-Jassim M. *Appl Phys Lett*, 2004, 85: 2625–2627
38 Dang XD, Tamayo AB, Seo J, Hoven CV, Walker B, Nguyen TQ. *Adv Funct Mater*, 2010, 20: 3314–3321
39 Chen HY, Lo MKF, Yang G, Monbouquette HG, Yang Y. *Nat Nanotechnol*, 2008, 3: 543–547
40 Li JB, Chawla V, Clemens BM. *Adv Mater*, 2012, 24: 720–723
41 Shin RH, Jo W, Kim DW, Yun J, Ahn S. *Appl Phys A*, 2011, 104: 1189–1194
42 Kim GY, Kim JR, Jo W, Son DH, Kim DH, Kang JK. *Nanoscale Res Lett*, 2004, 9: 10
43 Li J, Mitzi DB, Shenoy VB. *ACS Nano*, 2011, 5: 8613–8619
44 Yin WJ, Wu Y, Wei SH, Noufi R, Al-Jassim MM, Yan Y. *Adv Energy Mater*, 2014, 4: 1300712